Chapter 4
Normal Contact with Adhesion

Markus Heß and Valentin L. Popov

4.1 Introduction

The miniaturization of components and the manufacturing of ever smoother surfaces are a mark of the constant improvements in micro and nano-technologies today. For the length scales associated herewith, the adhesion forces must be doubtlessly taken into account. However, adhesion is also important for contacts in which one partner is composed of a very soft material. Above all, the adhesion between rough surfaces is a central research topic in this respect, as it deals with the friction of rubbers and the contact between biological structures.

From a theoretical point of view, one can name two main ansätze which were developed in order to describe adhesive contacts for *elastic*, parabolic bodies. The first is the theory of Johnson et al. [1] (JKR theory), which takes adhesion forces within the contact area into account. In this case, the contact radius in the equilibrium state is calculated from the minimum in the total energy, which in turn, is obtained from the elastic deformation energy, the potential of external forces, and the surface energy of the contacting bodies. On the other hand, in the theory developed by Derjagin et al. [2] (DMT theory), the molecular forces of attraction act only within a ring outside of the contact area. They naturally contribute to the normal force, however, it is assumed that they cause no deformation. Within the framework of DMT theory, the maximum magnitude of the adhesion force corresponds to that which Bradley derived in 1932 [3] for the adhesive contact between rigid spheres. Because the JKR theory diverges from the DMT theory, it appears at first that the two theories contradict each other. Tabor [4] was able to successfully explain this discrepancy by investigating the areas of validity of both theories in greater detail and defining them based on a dimensionless parameter. According to his findings, DMT theory is suitable for describing the contact of small, rigid spheres, while JKR theory is more adept at describing large, soft spheres. Johnson and Greenwood [5] created a map of adhesion, which graphically depicts the areas

V.L. Popov and M. Heß, *Method of Dimensionality Reduction in Contact Mechanics and Friction*, DOI 10.1007/978-3-642-53876-6_4

of validity for various adhesion theories. Furthermore, they pointed out the fact that the JKR theory still provides good results outside of its actual area of validity. It is possible that this is the reason that the JKR theory is primarily used to describe adhesion.

In this chapter, we will discuss how the leading adhesion theory from Johnson, Kendall, and Roberts is able to be exactly mapped using the method of dimensionality reduction. To begin, we will concentrate on a pure formulation of the simple rules of application for the adhesive normal contact and refrain from presenting the required evidence. Subsequently, these rules will be explained in more detail, which requires a certain understanding of the theoretical background on the adhesion in three-dimensional contacts, which we will also provide. For those not satisfied with these short explanations, the entirety of the necessary evidence may be found in Chap. 17.

4.2 Rule of Heß for the Adhesive Contact Between Axially-Symmetric Bodies

Adhesive contacts of axially-symmetric bodies can also be exactly mapped to a one-dimensional equivalent model. The rule for this mapping was developed by one of the authors (Heß) [6]. It is based on the basic idea of Johnson, Kendall, and Roberts that *the contact with adhesion arises from the contact without adhesion plus a rigid-body translation*. Because both parts of the contact problem can be mapped to a one-dimensional equivalent model with a modified geometry, then this is true of the entire problem. The rule of Heß is as follows: If an indenter with the modified form described in Chap. 3 is initially pressed into a linearly elastic foundation and then pulled out, as shown in Fig. 4.1, then the springs on the edge of the profile will detach upon reaching a critical length

$$\Delta\ell_{\max}(a) = \sqrt{\frac{2\pi a\,\Delta\gamma}{E^*}}, \tag{4.1}$$

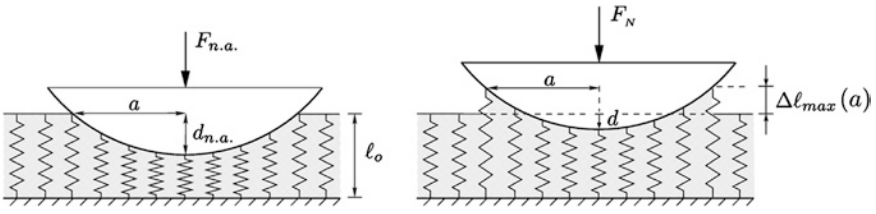

Fig. 4.1 Qualitative presentation of the indentation and separation process for the reduction method. The model shown exactly maps the adhesive contact of parabolic bodies and therefore, exactly mirrors JKR theory

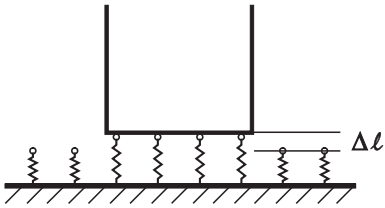

Fig. 4.2 Equivalent one-dimensional system for the adhesive contact between a flat, cylindrical indenter and an elastic half-space

where $\Delta\gamma$ is the separation energy of the bodies per unit area, which will be explained later in more detail. Here, it is worth noting that the separation criterion is not local, due to its dependence on the changing contact radius.

In order to illustrate the simple application of this rule, we will consider the adhesive contact between a flat, cylindrical indenter with the radius a and an elastic half-space (Fig. 4.2).

In this case, all springs will simultaneously detach as soon as the critical length (4.1) is reached. The total normal force required to separate the indenter from the substrate is then

$$F_A = 2E^* a\sqrt{\frac{2\pi a\,\Delta\gamma}{E^*}} = \sqrt{8\pi a^3 E^* \Delta\gamma}, \tag{4.2}$$

which corresponds exactly to the three-dimensional result [7]. For the problems at the end of this chapter, we will consider this type of contact problem once again by supplementing the general structure with relevant alterations. There, as well as in Sects. 4.4 and 4.5, there are numerous examples provided. However, before we proceed with these examples, we would like to explain the theoretical considerations that lead to Rule (4.1) in more detail. This is done primarily in Sect. 4.4, which contains further simple rules which help to determine the normal stress and the stability of the system. In this way, critical quantities can be determined very simply. We begin the theoretical consideration with the compatibility of the JKR theory with the ansätze from linear fracture mechanics. Those only interested in the practical application of the method of dimensionality reduction to adhesive contacts may continue directly with Sect. 4.4.

4.3 The Adhesive Contact and Griffith Crack

In the theory of Johnson, Kendall, and Roberts, the contact radius of an adhesive contact arises from the minimum total energy, which consists of the elastic deformation energy U_E, the potential of external forces U_P, and the surface energy U_S. In the original publication [1], it was already indicated that this energy ansatz is the same as that of Griffith [8, 9], which was once used to investigate fractures in

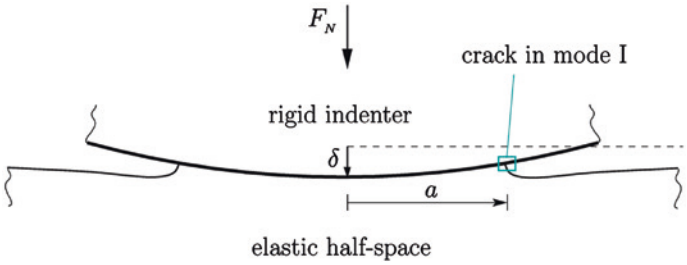

Fig. 4.3 Qualitative presentation of an adhesive contact between a rigid, curved body and an elastic half-space; the boundary of the contact can be referred to as the crack tip

brittle material[1] and is nothing more than the first law of thermodynamics. Maugis et al. [10, 11] conducted more penetrating thermodynamic considerations and proved, among other things, the compatibility of the JKR theory with that of linearly elastic fracture mechanics. The free boundary of the adhesive contact may, therefore, be referred to as a mode I crack,[2] which propagates either inwards or outwards based on changes in the contact surface. The decisive steps for the energy ansatz are very quickly explained. For this, we consider the adhesive contact between a rigid, curved body and an elastic half-space, according to Fig. 4.3. The indenter is loaded by an external force of F_N and, with the half-space, forms a contact area with a radius of a; in order to avoid confusion with differentials, the indentation depth will be denoted by δ in this section.

Initially, we assume that the indentation depth δ and the contact area A which describe the equilibrium state of the system are extensive properties. According to the first law of thermodynamics, a contribution of work from the external load, causes a change in the sum of the elastic deformation energy U_E and the surface energy U_S:

$$\mathrm{d}U_E(A,\delta) + \mathrm{d}U_S(A) = F_N(A,\delta)\mathrm{d}\delta. \tag{4.3}$$

The surface energy is not dependent on the indentation depth and is given by

$$U_S(A) = -\Delta\gamma \cdot A. \tag{4.4}$$

Here, $\Delta\gamma$ is the work that must be done per unit area against interatomic forces in order to separate the two solids, which is also known under the name of the Dupré energy of adhesion. It is dependent on the (specific) surface energies γ_1 and γ_2 of both bodies as well as the energy of the interface γ_{12}:

$$\Delta\gamma := \gamma_1 + \gamma_2 - \gamma_{12} \tag{4.5}$$

[1] More specifically, Griffith investigated the stability of a crack in the middle of a disc loaded in tension.

[2] The opening mode (mode I crack) is the separation mode for which the tensile stress acts *perpendicular* to the plane of the crack.

and can be interpreted as the "effective" interface energy. Insertion of (4.4) into (4.3) results in

$$\mathrm{d}U_E(A,\delta) - \Delta\gamma \cdot \mathrm{d}A = F_N(A,\delta)\ \mathrm{d}\delta. \tag{4.6}$$

By means of the Legèndre transformation, we can switch the independent extensive variables δ and F_N. In this way, we obtain

$$-\mathrm{d}U_E^K(A,F_N) - \Delta\gamma \cdot \mathrm{d}A = -\delta(A,F_N)\ \mathrm{d}F_N \quad \text{with} \quad U_E^K := F_N\delta - U_E, \tag{4.7}$$

in which U_E^K stands for the complementary elastic energy. By separating the total derivatives with respect to the corresponding variables, we obtain the laws of Castigliano and Engesser:

$$\left(\frac{\partial U_E}{\partial \delta}\right)_A = F_N \ \text{ or } \ \left(\frac{\partial U_E^K}{\partial F_N}\right)_A = \delta\,. \tag{4.8}$$

Furthermore, we now have two different possibilities for calculating the elastic energy release rate $\mathcal{G}$:

$$\mathcal{G} := \left(\frac{\partial U_E}{\partial A}\right)_\delta = -\left(\frac{\partial U_E^K}{\partial A}\right)_{F_N}. \tag{4.9}$$

In equilibrium, the mechanical energy released by a decrease in contact area must correspond to the energy required to form the new surface:

$$\mathcal{G} = \Delta\gamma =: \mathcal{G}_c. \tag{4.10}$$

Equation (4.10) once again provides the energetic fracture criterion of Griffith. Here, the effective interface energy $\Delta\gamma$ can be interpreted as the critical energy release rate $\mathcal{G}_c$ at which quasi-static fracture progression begins. The difference $\mathcal{G} - \Delta\gamma$ is occasionally called the *driving force* (with the units of linear force density) for the tip of the fracture and allows for the kinetic adhesive process to be investigated.

The energetic fracture criterion from Griffith in the form of (4.10) contains the energy release rate as a parameter and, as a result, is seen as a *global* fracture criterion. An equivalent criterion, and for our purposes more appropriate due to its *local* characteristic, is found using the concept of stress intensity. Irwin [12] recognized the fundamental fact that the singularities of all stress fields for all fracture types are similar in the fracture near field, and therefore, used their intensities for the investigation of fracture mechanics. The ligament stresses and the displacements which exist, for example, in the near field of the fracture shown in Fig. 4.4 with the separation mode I are

$$\sigma_{zz}(\eta,\beta=0) = \frac{K_I}{\sqrt{2\pi\eta}} \ \text{ and } \ u_z(\eta,\beta=\pm\pi) = \pm\frac{2}{E^*}K_I\sqrt{\frac{\eta}{2\pi}}\,. \tag{4.11}$$

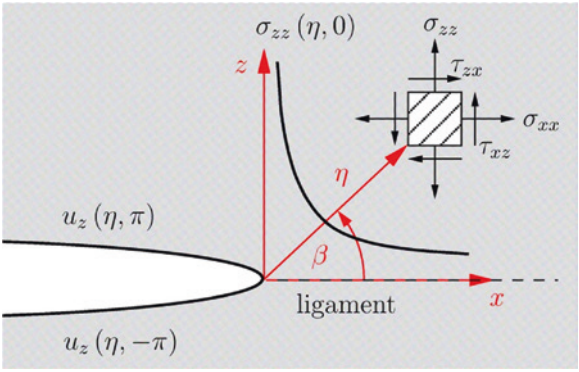

Fig. 4.4 Qualitative presentation of the ligament stress and the opening form of a mode I crack

The stress intensity factor K_I, which is dependent on the material as well as the geometry, length, and loading of the fracture, can be obtained if the ligament stress is known:

$$K_I := \lim_{\eta \to 0} \sqrt{2\pi\eta}\, \sigma_{zz}(\eta, 0). \tag{4.12}$$

According to Irwin, fracture propagation occurs only after K_I reaches the so-called fracture toughness K_{Ic} of the material, which must, in turn, be determined experimentally on standardized fracture experiments. Therefore, the *local* fracture criterion from Irwin for a mode I crack is

$$K_I = K_{Ic}. \tag{4.13}$$

Of course, no real material can withstand the (theoretically) infinitely large stress. Except for very brittle materials, a relaxation in stress occurs in the area near the fracture tip due to inelastic deformation. Furthermore, regardless of the material, a small zone always exists in which non-linear microscopic processes occur. As long as the combination of the plastic and microscopic zones is much smaller than the zone in which K_I dominates, the elastic near field will control the processes occurring in this field, allowing the use of the concept of stress intensity. The fact that the K concept and the fracture criterion from Griffith are equivalent was proven by Irwin for which he calculated the work required to close a fracture of length Δa[3]:

$$\mathcal{G} = \frac{K_I^2}{2E^*}. \tag{4.14}$$

Equation (4.14) is for a mode I crack. If a combined fracture load is present for which all three separation modes occur, then the individual energy release rates

[3] The equation is based on a fracture in a planar state of deformation; we may assume that locally in an axially-symmetric contact with adhesion, every point on the contact boundary exhibits this state.

must be summed. In the case of a fracture interface between two elastically similar materials, the following is then valid:

$$\mathcal{G} = \frac{1}{2E^*}\left(K_I^2 + K_{II}^2\right) + \frac{1}{4}\left(\frac{1}{G_1} + \frac{1}{G_2}\right)K_{III}^2. \tag{4.15}$$

With the help of this generalized presentation, the interaction between adhesion and friction can be determined [13].

It may have been the equivalence of the concepts of the fracture mechanism that motivated Maugis and Barquins [14, 15] to use Sneddons theory [16] for the mapping of adhesive contacts; the analogy between JKR theory and the Griffith theory of fracture mechanics was already proven at this time. Thus, the concept of the stress intensity factor must also exist in Sneddons theory. The original equations from Sneddon contain a (still arbitrary) rigid body translation, which is responsible for a singularity in the stress at the contact boundary. The translation is that which results from pressing a flat cylindrical indenter into a half-space and corresponds to that of the initial approximation for a mode I crack. Furthermore, the difference in the normal displacement between the indenter and surface of the half-space outside of the contact area is the same as the shape of the fracture in Eq. (4.11), so that a connection exists between the rigid body degree of freedom and the intensity factor. For contacts without adhesion, with the assumption that the profile is convex, the Boussinesq condition must be met, meaning that the singularity at the contact boundary disappears. The only difference between the two theories is the rigid body translation. This causes a tensile stress for which the distribution is the same as that under a flat cylindrical indenter. This is an essential relationship, which we would like to stress:

> *The contact with adhesion results from the contact without adhesion plus a rigid body translation.*

Even the original theory of Johnson, Kendall, and Roberts touches on this principle, which extends the Hertzian contact by adding adhesion. This theory was discussed in a generalized form at the beginning of this chapter. It requires, among other things, that the energy of the elastic deformation be known, which in turn, can be determined in two parts. One of these comes from the non-adhesive indentation process, while the other results from the decompression at a constant contact area. Figure 4.5 explains the superposition of the two loading cases. The indentation process with a force $F_{n.a.}$ occurs without adhesion, so that the resulting stresses and surface displacements are for a Hertzian contact. Due to the successive increase in the relative interface energy, the subsequent unloading from $F_{n.a.}$ to F_N occurs for a constant contact area. Because of this, all points in the contact area must undergo a constant displacement. Therefore, the unloading is the same as for the contact with a flat indenter, the characteristic stress distribution for which is responsible for the infinitely large tensile stress at the contact boundary.

This singularity can be seen in Fig. 4.5b, the stresses for which are shown with respect to their mean in the non-adhesive contact. Interestingly, Johnson [17] had already recognized the ability to use superposition to describe a contact with adhesion in 1958. The non-physical excess in stress on the boundary, however, led him

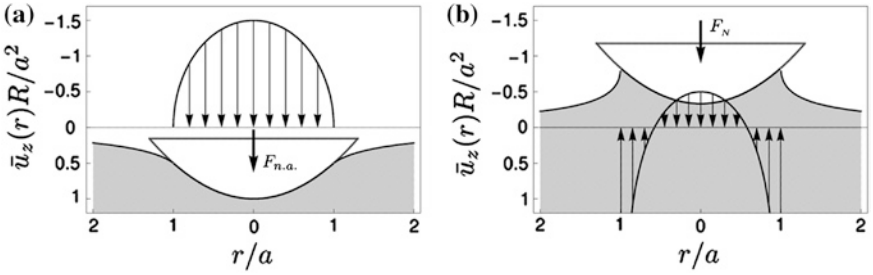

Fig. 4.5 **a** Hertzian spherical contact caused by the normal force $F_{n.a.}$, which leads to the same contact radius as in the adhesive case under the load of F_N; **b** Equilibrium state of the adhesive contact; more exactly, the critical state under a *fixed-load* condition is actually shown here

to *rule out* adhesion, which was in accord with the experimental works of Bowden and Tabor at the time.

4.4 Full Reduction of the Adhesive, Elastic Contact

The central notion of the exact mapping of axially-symmetric contacts with adhesion is the superposition concept described in the last section. According to this, the contact without adhesion must merely be superimposed with a rigid body translation. This means that the normal stress distribution in the contact area is

$$\sigma_{zz}(r) = \sigma_{n.a.}(r) + \frac{\Delta F}{2\pi a\sqrt{a^2 - r^2}} \quad \text{with} \quad \Delta F := F_{n.a.} - F_N = 2E^* a(d_{n.a.} - d), \tag{4.16}$$

where the second term is the stress distribution under a flat indenter described by Boussinesq. Remember that the values with the index "n.a." are those for a contact without adhesion for which the same contact radius is reached as that in a contact with adhesion. They belong to the (fictitious) indentation process for the JKR theory, which was shown in Fig. 4.5a. The stress intensity factor for the distribution in (4.16) can be easily calculated using Eq. (4.12):

$$K_I(a) = \frac{\Delta F}{2a\sqrt{\pi a}}. \tag{4.17}$$

By taking into consideration the fact that the concepts of Griffith and Irwin (4.14) are equivalent and that the equilibrium condition (4.10) is met, then

$$\Delta F = \sqrt{8\pi E^* a^3 \Delta\gamma}, \tag{4.18}$$

with which the indentation depth and the normal force can be directly determined for the adhesive case:

$$d(a) = d_{n.a.}(a) - \sqrt{\frac{2\pi a\,\Delta\gamma}{E^*}}, \tag{4.19}$$

$$F_N(a) = F_{n.a.}(a) - \sqrt{8\pi E^* a^3 \Delta\gamma}. \tag{4.20}$$

The validity of Eqs. (4.19) and (4.20) is in no way limited to the parabolic contact. They are generally valid for arbitrary axially-symmetric contacts with a simply connected contact area [18].

No additional proof is needed to show that the results of the generalized JKR theory can be mapped to one-dimensional models. This is because if arbitrary axially-symmetric contacts without adhesion (for simply connected contact areas) satisfy the requirements of the reduction method (see Chap. 3), including the flat indenter, then this must also be true for their superposition. The adhesive contact forms a sort of special case of the rule of superposition described in Sect. 3.2, which is valid for the same contact areas. Nevertheless, Sect. 17.3 contains a step-by-step derivation, including information dealing with stability, which is based on the fracture mechanical analogy found by Maugis and Barquins.

The model for the adhesive contact between a parabolic indenter and an elastic half-space is sketched in Fig. 4.1. The loading and unloading process for the one-dimensional model, which exactly describes the equilibrium state of the adhesive contact in three dimensions, is simple. As in the case without adhesion, the equivalent profile g is first calculated and an appropriately formed indenter is subsequently pressed into a one-dimensional linearly elastic foundation with a force $F_{n.a.}$. The springs at the contact boundary $x = \pm a$ exhibit the non-loaded initial length ℓ_o, while the springs within the contact area are under load. Let us now assume that all springs in contact with the indenter adhere to it and for a subsequent decrease in normal force, the contact radius remains unchanged. Going from the contact boundary towards the center, more and more springs are placed under tensile loading. As soon as the change in length of the outer springs reach the maximum allowable value

$$\Delta\ell(\pm a) = \Delta\ell_{\max}(a) := \sqrt{\frac{2\pi a\,\Delta\gamma}{E^*}}, \tag{4.21}$$

there exists an indifference between the states of adhesion and separation. At the points $x = \pm a$, the surface displacement for the one-dimensional model is

$$u_z(\pm a) = -\Delta\ell_{\max}(a). \tag{4.22}$$

This state corresponds exactly to that of the equilibrium state in the three-dimensional case of adhesive contact. The separation condition (4.21) is a type of *local* fracture criterion for the equivalent model, which is also known as the

rule of Heß for the adhesive contact [6, 19]. Alternately, we can define a maximum spring force instead of a maximum change in length. Upon exceeding this force, the springs at the boundary separate. Especially for the numerical application, the dependence of the separation condition on the contact half-width should be taken into account.

Even the stability of the equilibrium state can be investigated very trivially under various boundary conditions within the framework of the reduction method. For this (referring to Sect. 17.3), the following inequality is used:

$$\frac{\Delta\ell_{\max}(a)}{a} \leq k\frac{\partial g(a)}{\partial a} \quad \text{with } k = \begin{cases} 2/3 & \text{for } F_N = const. \\ 2 & \text{for } d = const. \end{cases} . \tag{4.23}$$

The equals sign in (4.23) defines the state of marginal stability, which allows for the critical values to be calculated. According to (4.23), the slope of the equivalent profile at the point $x = a$ determines the stability of the system. Depending on the boundary condition (*fixed-load* or *fixed-grips*), it is to be multiplied with the corresponding factor k and compared with the quotient of the separation length and contact radius.

With the exception of the stability considerations named above, the implementation of adhesion using the reduction method requires no additional effort whatsoever. In contrast to the non-adhesive contact, only the displacement in the one-dimensional model must be extended by the rigid-body portion (see Fig. 4.1)

$$u_z(x) := d(a) - g(x) = g(a) - g(x) - \Delta\ell_{\max}(a) \quad \text{for } 0 \leq |x| \leq a. \tag{4.24}$$

The indentation depth is defined by the displacement at $x = 0$:

$$d(a) := u_z(0) = g(a) - \Delta\ell_{\max}(a). \tag{4.25}$$

By taking (4.24) and (4.25) into account, the normal force is obtained as a function of the contact radius in the same way as before, from the sum of the spring forces:

$$F_N(a) := E^* \int_{-a}^{a} u_z(x)\mathrm{d}x. \tag{4.26}$$

The normal stresses in the contact area are obtained also in the same way as in the contact without adhesion, from the modified Abel integral of the vertical distributed load:

$$\sigma_{zz}(r) = \frac{1}{\pi}\int_r^a \frac{q'(x)}{\sqrt{x^2 - r^2}}\,\mathrm{d}x - \frac{1}{\pi}\frac{q(a)}{\sqrt{a^2 - r^2}} \quad \text{with} \quad q(x) = E^* u_z(x). \tag{4.27}$$

In order to make the simple steps of the reduction method clear to the reader, we will show the complete mapping of the original theory from Johnson, Kendall, and Roberts as an example. In the typical way, the equivalent profile g of the parabolic

indenters with the radius of curvature must first be determined. According to the *rule of Popov*, we must simply divide the radius of curvature by two:

$$f(r) = \frac{r^2}{2R} \Rightarrow g(x) = \frac{x^2}{R} \cdot \tag{4.28}$$

The surface displacement in the equivalent model, according to Eq. (4.24), is

$$u_z(x) = \frac{a^2 - x^2}{R} - \Delta\ell_{\max}(a), \tag{4.29}$$

from which we can determine the indentation depth with respect to contact radius according to (4.25). Taking the separation condition (4.21) into account, we obtain

$$d(a) = \frac{a^2}{R} - \sqrt{\frac{2\pi a\,\Delta\gamma}{E^*}}. \tag{4.30}$$

The normal force is the sum of the spring forces

$$F_N(a) = E^* \int_{-a}^{a} u_z(x)\mathrm{d}x = 2E^* \int_{0}^{a} \left(d - \frac{x^2}{R}\right)\mathrm{d}x = \frac{4}{3}E^*\frac{a^3}{R} - \sqrt{8\pi a^3 E^* \Delta\gamma}. \tag{4.31}$$

Equations (4.30) and (4.31) will seem familiar to the reader, for they are exactly those developed by Johnson, Kendall, and Roberts using the minimum in the total energy.

We investigate the stability of the system with the criterion (4.23). For this, let k not be fixed for the time being. The slope of the equivalent profile at the point $x = a$ is

$$g(a) = \frac{a^2}{R} \Rightarrow \frac{\partial g(a)}{\partial a} = \frac{2a}{R}. \tag{4.32}$$

Insertion of (4.32) into (4.23) and taking the separation condition (4.21) into account, results in

$$\sqrt{\frac{2\pi a\,\Delta\gamma}{E^*}}\frac{1}{a} \leq k\frac{2a}{R}, \tag{4.33}$$

and after simple rearrangement, the contact radii for which the system is stable are obtained:

$$a \geq \left(\frac{\pi R^2 \Delta\gamma}{2k^2 E^*}\right)^{1/3} \quad \text{marginal stability: } a_c(k) = \left(\frac{\pi R^2 \Delta\gamma}{2k^2 E^*}\right)^{1/3}. \tag{4.34}$$

The marginally stable case characterizes the critical state at which the calculation of the critical values is possible: the minimum normal force and minimum indentation depth. In order to accomplish this, the contact radius in Eq. (4.34) must be take into account in Eqs. (4.30) and (4.31), from which we obtain

$$F_c(k) = \left(\frac{1}{3k} - 1\right)\frac{2\pi R\,\Delta\gamma}{k} \text{ and } d_c(k) = \left(\frac{1}{k} - 2\right)\left(\frac{\pi^2 R\,\Delta\gamma^2}{4k\,E^{*^2}}\right)^{1/3}. \tag{4.35}$$

Until now, we have left the type of boundary condition open. Now, we will assign the variable k a value. Under the *fixed-load* condition, we must set $k = \frac{2}{3}$ and obtain the known results:

$$a_c = \left(\frac{9\pi R^2 \Delta\gamma}{8E^*}\right)^{1/3}, \; F_c = -\tfrac{3}{2}\pi R\,\Delta\gamma\,, \; d_c = -\left(\frac{3\pi^2 R\,\Delta\gamma^2}{64E^{*2}}\right)^{1/3}. \quad (4.36)$$

The critical force in (4.36) is also called the *adhesion force* and corresponds to the minimum in the normal force. Its magnitude, however, is called the *maximum separation force.* Under the *fixed-grips* condition ($k = 2$), the indentation depth is actually able to be *stably* decreased even further, until the following three relationships are reached:

$$a_{c,d} = \left(\frac{\pi R^2 \Delta\gamma}{8E^*}\right)^{1/3}, \; F_{c,d} = -\tfrac{5}{6}\pi R\,\Delta\gamma\,, \; d_{c,d} = -\tfrac{3}{4}\left(\frac{\pi^2 R\,\Delta\gamma^2}{E^{*2}}\right)^{1/3}, \quad (4.37)$$

The additional index "d" denotes the fixed-grips condition.

For the sake of completeness, let the equilibrium curves (4.30) and (4.31) be expanded by a normalized representation. With the respect to the magnitude, the critical values are

$$\tilde{F}_N(\tilde{a}) = \tilde{a}^3 - 2\tilde{a}^{3/2} \text{ and } \tilde{d}(\tilde{a}) = 3\tilde{a}^2 - 4\tilde{a}^{1/2}, \quad (4.38)$$

with $\tilde{F}_N := F_N/|F_c|$, $\tilde{d} := d/|d_c|$, and $\tilde{a} := a/a_c$. Because of their complexity due to the normal force as a function of the indentation depth, they will not be specified explicitly, but their trends will be graphically shown with the help of the parametric form (4.38). Figure 4.6a shows the trend compared to the adhesive contact of a conical profile (shown in Fig. 4.6b). The dashed ends of the functions mark the extended domain of stability under the *fixed-grips* condition.

Comparing the curves reveals that the adhesion forces are negative in both cases, but the critical indentation depths (at a constant force) have different signs. The solution of the adhesive conical contact and the confirmation of the corresponding curves from Fig. 4.6b is one of the problems at the end of this chapter.

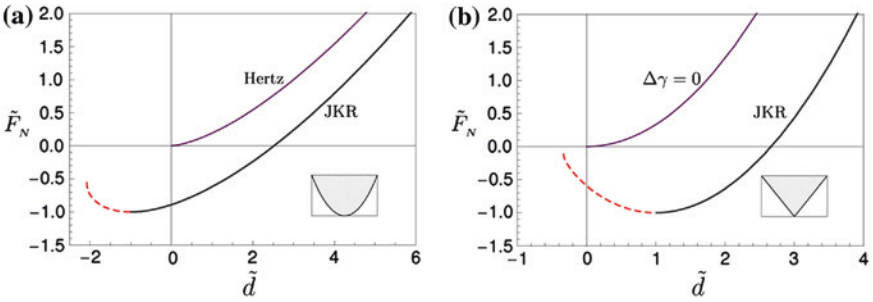

Fig. 4.6 Dependence of the normalized force on the normalized indentation depth for the adhesive contact for a parabolic (**a**) and a conical indenter (**b**); for comparison purposes, the trends of the respective contacts without adhesion are shown

Only the calculation of the stress is now needed to completely solve the adhesive contact problem for parabolic profiles. For this, we need the linear force density in the equivalent model:

$$q(x) = E^* u_z(x) = E^* \left[\frac{a^2 - x^2}{R} - \Delta\ell_{\max}(a) \right]. \tag{4.39}$$

By differentiating this with respect to x and then inserting the value at $x = a$, we obtain

$$q'(x) = -\frac{2E^*}{R} x \text{ and } q(a) = -E^* \Delta\ell_{\max}(a)\,. \tag{4.40}$$

Insertion of (4.40) into (4.27) results initially in

$$\sigma_{zz}(r) = -\frac{2E^*}{\pi R} \int_r^a \frac{x}{\sqrt{x^2 - r^2}}\,\mathrm{d}x + \frac{E^*}{\pi} \frac{\Delta\ell_{\max}(a)}{\sqrt{a^2 - r^2}}, \tag{4.41}$$

which is then integrated and suitably normalized, resulting in

$$\frac{\sigma_{zz}(s)}{\bar{p}_{n.a.}} = -\frac{3}{2}\sqrt{1 - s^2} + \frac{1}{2}\left(1 - \frac{F_N}{F_{n.a.}}\right) \frac{1}{\sqrt{1 - s^2}} \text{ with } s := \frac{r}{a} \text{ and } \bar{p}_{n.a.} := \frac{F_{n.a.}}{A}\,. \tag{4.42}$$

For the critical state of $F_c := F_N(a_c) = -F_{n.a.}$, this stress curve is presented in Fig. 4.5b.

The process for mapping the classical contact problems described by Johnson, Kendall, and Roberts within the reduction method may seem a bit challenging at first. However, the reader will quickly be convinced that, in reality, the opposite is the case. The method is composed primarily of just a few steps, which are formulated in Eqs. (4.21)–(4.27) and cannot be simpler. In the next section, the method will be used on a more complicated contact problem, which occasionally allows for commentary on the influence of roughness on adhesion.

4.5 Example: Adhesion of a Sphere with a Superimposed Radial Waveform

It is generally known that the adhesion between (visco-) elastic bodies is significantly influenced by the roughness of their surfaces. In the most general cases, the adhesion decreases rapidly with an increase in roughness, however, there are well-founded experimental results [20, 21], which show effects to the contrary. According to this, very soft materials having small scales of roughness exhibit a temporary increase in adhesion before a continuous decrease begins. An established theoretical reason for this increase is based on the increase in the real contact area, which occurs due to viscoelastic creep processes. A further cause for the increase in adhesion was brought to attention by Guduru [22] by theoretically

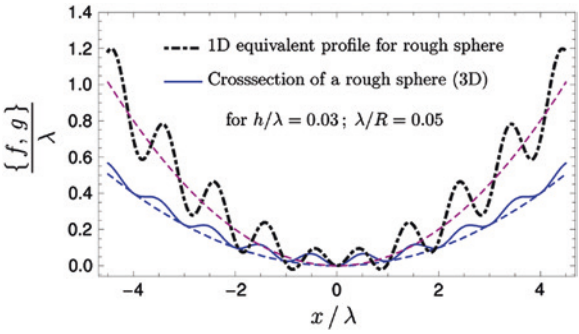

Fig. 4.7 Profile cross-section of a parabolic body superimposed with a radial waveform and its one-dimensional equivalent

investigating the adhesive, elastic contact between a half-space and a parabolic body with superimposed axially-symmetric waveforms. Due to the waveform, defined oscillations occur in the equilibrium curves, bringing about instabilities during the separation process. These instabilities can lead to a significant increase in the separation force. Experimental investigations [23] confirm the validity of the theoretical ansatz from Guduru, which requires a simply connected contact area at the beginning of the separation process. This last condition, along with that of axial-symmetry, allow this example for a rough contact to be *exactly* mapped using the method of dimensionality reduction, which will be the subject of the following considerations.

The axially-symmetric profile is composed of a parabolic base profile with a radius of curvature of R and a radially harmonic profile with the wavelength λ and the (roughness) amplitude h according to the equation[4]

$$f(r) = \frac{r^2}{2R} + h\left[1 - \cos\left(\frac{2\pi}{\lambda}r\right)\right]. \tag{4.43}$$

The cross-section of the profile in the x-z plane for $h/\lambda = 0.03$ and $\lambda/R = 0.05$ is shown in Fig. 4.7. A simply connected contact area at *every* point in time for the indentation and separation process requires a monotonically increasing profile for $r \geq 0$, which with the help of the derivative

$$f'(r) = \frac{r}{R} + h\frac{2\pi}{\lambda}\sin\left(\frac{2\pi}{\lambda}r\right), \tag{4.44}$$

is expressed by the following condition:

$$f'(r) \geq 0 \Rightarrow \alpha := \frac{\lambda^2}{hR} \geq 4\pi^2 \sup\left[\frac{-\sin\left(\frac{2\pi}{\lambda}r\right)}{\frac{2\pi}{\lambda}r}\right] \approx 8.576. \tag{4.45}$$

[4] It is irrelevant if the superimposed profile is pressed into a planar elastic half-space or a parabolic body is pressed into an elastic half-space with the corresponding waveform.

Although the monotonic requirement (4.45) is obviously not met by the profile in Fig. 4.7 ($\alpha \approx 1.667 < 8.576$), a simply connected contact area can nevertheless be realized for a sufficiently large normal force. The reason for this is the decrease in the least upper bound (supremum) in (4.45), if we constrict ourselves to sufficiently large $r > r_{crit}$.

In order to determine the one-dimensional equivalent profile, we must make use of the conversion formula (see Sect. 3.3).

$$g(x) := |x| \int_0^{|x|} \frac{f'(r)}{\sqrt{x^2 - r^2}} \mathrm{d}r = \frac{x^2}{R} + s(x)h \int_0^{s(x)} \frac{\sin(u)}{\sqrt{s(x)^2 - u^2}} \mathrm{d}u \quad \text{with} \quad s(x) = \frac{2\pi}{\lambda}|x|. \tag{4.46}$$

The integral on the right side leads to the Struve function, so that we obtain

$$g(x) = \frac{x^2}{R} + \frac{\pi^2}{\lambda}|x|h \cdot H_0\left(\frac{2\pi}{\lambda}|x|\right) \tag{4.47}$$

for the equivalent profile. Let us here mention that the series representation of the Struve function is

$$H_n(x) = \sum_{k=0}^{\infty} \frac{(-1)^k}{\Gamma\left(k + \frac{3}{2}\right)\Gamma\left(k + n + \frac{3}{2}\right)} \left(\frac{x}{2}\right)^{2k+n+1}. \tag{4.48}$$

The one-dimensional equivalent profile according to Eq. (4.47) is likewise presented in Fig. 4.7. Moreover, the original and equivalent profiles are shown for a roughness of zero (dashed lines) and present, of course, a constant vertical scaling relationship based on the rule of Popov.

Upon obtaining the one-dimensional profile, the three-dimensional problem is as good as solved, because now the modified profile must simply be pressed with sufficient force into the one-dimensional layer of springs and then the force reduced while taking the equilibrium condition (4.22) and the accompanying stability test (4.23) into account. The numerical implementation is trivial due to the independence of the spring displacement, but nevertheless, agrees exactly with the three-dimensional theory! In the following, we conduct an analytical approach, which leads to the indentation depth when Eq. (4.47) is taken into account:

$$d(a) := g(a) - \Delta\ell_{\max}(a) = \frac{a^2}{R} + \frac{\pi^2 ah}{\lambda} H_0\left(\frac{2\pi}{\lambda}a\right) - \sqrt{\frac{2\pi a\,\Delta\gamma}{E^*}}. \tag{4.49}$$

The surface displacement of the linearly elastic foundation is defined by the difference between the indentation depth d and the equivalent profile g. Except for

the sign, this displacement corresponds to the change in length of the springs. The resulting spring forces must maintain equilibrium by summation with the normal force:

$$F_N(a) = E^* \int_{-a}^{a} \big[d - g(x)\big]\,\mathrm{d}x. \tag{4.50}$$

Insertion of (4.47) and (4.49) into (4.50) results in

$$F_N(a) = \frac{4}{3}E^*\frac{a^3}{R} + E^*\pi a h\left[\frac{2\pi a}{\lambda}H_0\left(\frac{2\pi a}{\lambda}\right) - H_1\left(\frac{2\pi a}{\lambda}\right)\right] - \sqrt{8\pi a^3 E^* \Delta\gamma} \tag{4.51}$$

after integration and simple rearrangement. By taking the normalized values suggested by Guduru [22] into account:

$$\bar{F}_N := \frac{2F_N}{3\pi R\Delta\gamma}\,,\ \bar{d} := \frac{d}{\lambda}\,,\ \bar{a} := \frac{a}{\lambda}\,,\ \bar{\lambda} := \frac{\lambda}{R}\,,\ \bar{h} := \frac{h}{\lambda}\,,\ \overline{\Delta\gamma} := \frac{2\pi\Delta\gamma}{E^*R}$$

the equilibrium relations (4.49) and (4.51) can be expressed in dimensionless form:

$$\bar{d}\left(\bar{a};\bar{\lambda};\bar{h};\overline{\Delta\gamma}\right) = \bar{a}^2\bar{\lambda} + \pi^2\bar{a}\,\bar{h}\cdot H_0(2\pi\bar{a}) - \sqrt{\frac{\bar{a}\,\overline{\Delta\gamma}}{\bar{\lambda}}}, \tag{4.52}$$

$$\bar{F}_N\left(\bar{a};\bar{\lambda};\bar{h};\overline{\Delta\gamma}\right) = \frac{16}{9}\frac{\bar{a}^3\bar{\lambda}^3}{\overline{\Delta\gamma}} + \frac{4\pi}{3}\frac{\bar{a}\,\bar{h}\bar{\lambda}^2}{\overline{\Delta\gamma}}[2\pi\bar{a}\cdot H_0(2\pi\bar{a}) - H_1(2\pi\bar{a})] - \frac{8}{3}\sqrt{\frac{\bar{a}^3\bar{\lambda}^3}{\overline{\Delta\gamma}}}. \tag{4.53}$$

With the normalized contact radius $\bar{a}$ as a parameter, the (normalized) normal force can be plotted as a function of the (normalized) indentation depth. Figure 4.8 shows this plot for the parameters

$$\bar{h} = 0.005\,,\ \bar{\lambda} = 0.05\,,\ \overline{\Delta\gamma} = 0.05, \tag{4.54}$$

which only exhibits slight oscillating deviations in the equilibrium curve compared to the parabolic contact without roughness. The monotonic condition (4.45) is satisfied regardless of the load at any point in time.

If we now increase the size of the roughness and keep all other values the same, then a significant change occurs in the equilibrium curve. Oscillations of strong amplitude occur and can lead to an increase in the maximum separation force. Figure 4.9 presents this curve for the profile discussed at the beginning of this section (see Fig. 4.7), which is characterized by a roughness six times larger. The maximum separation force is increased by about 19 % with respect to the parabolic base profile. The critical indentation depth can be decreased by a further 10 % by using the fixed grips condition. Furthermore, the equilibrium curves are

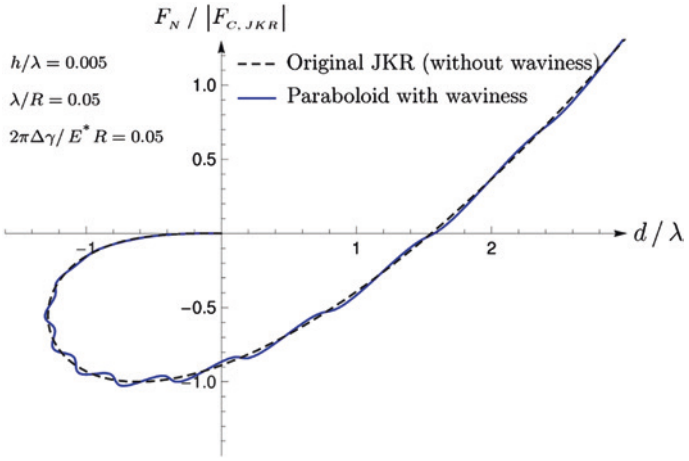

Fig. 4.8 Normal force with respect to the indentation depth for the adhesive contact of a parabolic profile with a superimposed radial waveform. The (small) roughness $h = 0.005\,\lambda$ causes only a minor difference from the original trend of the JKR theory

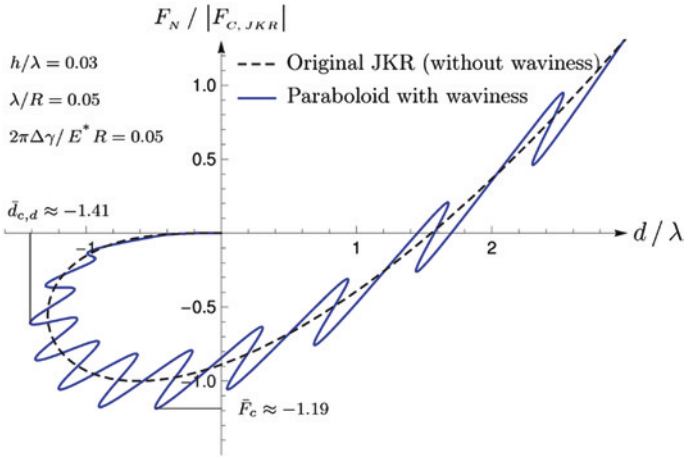

Fig. 4.9 Normal force with respect to the indentation depth for the adhesive contact with a superimposed radial waveform. The assumed roughness of $h = 0.03\,\lambda$ causes strong oscillations, resulting in an additional increase in the adhesion force of about 19 % compared to the original JKR theory

not continuous throughout the separation process. Due to the constant switching from stable to unstable domains, finite jumps occur, which result in energy loss.

As mentioned earlier, the exact solution of contact problems using the method of dimensionality reduction requires a simply-connected contact area and cannot be immediately transferred to partial contacts. Furthermore, the superimposed

waveforms must be axially-symmetric. If one of these requirements is not met, significantly divergent results can result. For example, if a planar waveform instead of a radial waveform is present, then there will be no jumps in the equilibrium curve [24].

4.6 Problems

Problem 1 Investigate the contact between an elastic half-space and a conical body defined by $f(r) = \tan\theta \cdot r$. Adhesion forces should be taken into account. Determine the indentation depth and the normal force with respect to the contact radius. Furthermore, determine the critical values under the *fixed-load* conditions and the equilibrium relations in dimensionless parameters.

Solution The equivalent one-dimensional profile is obtained by vertically scaling the original profile by a factor of $\kappa_1 = \pi/2$ and is equal to $g(x) = (\pi/2)\tan\theta \cdot |x|$. From (4.24), the surface displacement can be obtained for the equivalent profile:

$$u_z(x) = g(a) - g(x) - \Delta\ell_{\max}(a) = \frac{\pi}{2}\tan\theta \cdot (a - |x|) - \Delta\ell_{\max}(a). \tag{4.55}$$

The indentation depth is the displacement at the point $x = 0$:

$$d(a) := u_z(0) = \frac{\pi}{2}\tan\theta \cdot a - \Delta\ell_{\max}(a) = \frac{\pi}{2}\tan\theta \cdot a - \sqrt{\frac{2\pi a\,\Delta\gamma}{E^*}}. \tag{4.56}$$

The sum of the spring forces must counteract the normal force:

$$F_N(a) = E^* \int_{-a}^{a} u_z(x)\mathrm{d}x = 2E^* \int_{0}^{a} \big[d - g(x)\big]\mathrm{d}x = \frac{1}{2}\pi E^* \tan\theta \cdot a^2 - \sqrt{8\pi a^3 E^* \Delta\gamma}. \tag{4.57}$$

We take the condition for calculating the critical contact radius a_c at a constant contact radius from Eq. (4.23):

$$\frac{\Delta\ell_{\max}(a_c)}{a_c} = \frac{2}{3}\frac{\partial g(a)}{\partial a}\bigg|_{a=a_c} \quad \text{with} \quad \frac{\partial g(a)}{\partial a} = \frac{\pi}{2}\tan\theta\,, \tag{4.58}$$

for which the right hand side is already extended by the slope of the profile at hand. By using the rule of Heß, the critical contact radius is obtained. Insertion of this value into the equilibrium relationships (4.56) and (4.57) and then rearranging the equations results in the adhesion force and the critical indentation depth:

$$a_c = \frac{18\,\Delta\gamma}{\pi\tan^2\theta \cdot E^*},\; F_c = -\frac{54\,\Delta\gamma^2}{\pi\tan^3\theta \cdot E^*},\; d_c = \frac{3\,\Delta\gamma}{\tan\theta \cdot E^*}\cdot \tag{4.59}$$

By introducing the normalized values $\tilde{F}_N := F_N/|F_c|$, $\tilde{d} := d/|d_c|$, and $\tilde{a} := a/a_c$, we obtain the equilibrium relationships (4.56) and (4.57) in dimensionless form:

$$\tilde{F}_N(\tilde{a}) = 3\tilde{a}^2 - 4\tilde{a}^{3/2} \text{ and } \tilde{d}(\tilde{a}) = 3\tilde{a} - 2\tilde{a}^{1/2}. \tag{4.60}$$

With the help of the parametric equations in (4.60), the normalized force can be easily plotted as a function of normalized indentation depth, which is shown in Fig. 4.6b. The comparison with the parabolic contact shows, above all, a striking difference in the critical indentation depth (under *fixed-load* conditions), which have opposing signs. All of the results for this exercise mirror the three-dimensional theory exactly (see [14]).

Problem 2 Determine the maximum separation force for the elastic contact between a flat, cylindrical indenter with the radius a and a half-space.

Solution From the original profile $\mathrm{f}(r) = 0$, the equivalent profile $g(x) = 0$ is directly obtained, so that the surface displacement within the contact area corresponds everywhere to the indentation depth according to (4.24). This means that

$$u_z(x) = d(a) = -\Delta\ell_{\max}(a) = -\sqrt{\frac{2\pi a\,\Delta\gamma}{E^*}}\,. \tag{4.61}$$

Because all of the springs exhibit the same change in length based on (4.61), the calculation of the normal force is trivial:

$$F_N(a) = -2E^* a\,\Delta\ell_{\max}(a) = -\sqrt{8\pi a^3 E^* \Delta\gamma}. \tag{4.62}$$

The verification of the condition (4.23), however, uncovers the fact that a stable, quasi-static equilibrium in the form of a controlled fracture is not possible. Therefore, all of the springs will adhere to the indenter until they reach the change in length of (4.61) and then simultaneously separate (*complete rupture)*. The normal force according to (4.62) presents simultaneously the adhesion force and the magnitude of the maximum separation force

$$F_A := |F_N(a_c)| = \sqrt{8\pi a^3 E^* \Delta\gamma}, \tag{4.63}$$

which corresponds with the known result of Kendall [7].

Problem 3 Analyze the influence of the profile form on the adhesion force for a single contact within a biological system. For this, assume an axially-symmetric profile in the form of a power function with a positive real exponent according to

$$f(r) = C \cdot r^n \text{ with } n \in \mathbb{R}^+\,. \tag{4.64}$$

In the first step, identify the equilibrium relationships $F_N(a)$ and $d(a)$. Then, calculate the critical values for marginal stability from (4.23) for a *constant normal force* and non-dimensionalize the equilibrium relationships.

Solution We obtain the one-dimensional equivalent profile by using the generalized rule of Heß (see Sect. 3.2):

$$g(x) = \kappa_n f(|x|) = \kappa_n C|x|^n \text{ with } \kappa_n = \frac{\sqrt{\pi}}{2}\frac{n\Gamma(\frac{n}{2})}{\Gamma(\frac{n+1}{2})}. \tag{4.65}$$

The difference between the value of the function for the equivalent profile at the contact boundary and the separation length provides the indentation depth

$$d(a) = g(a) - \Delta\ell_{\max}(a) = \kappa_n C a^n - \sqrt{\frac{2\pi a\,\Delta\gamma}{E^*}}. \tag{4.66}$$

The surface displacement in the one-dimensional model is then

$$u_z(x) := d - g(x) = \kappa_n C\left(a^n - |x|^n\right) - \sqrt{\frac{2\pi a\,\Delta\gamma}{E^*}}, \tag{4.67}$$

which expresses, except for the sign, the change in length of the individual springs. After multiplication with the stiffness and summation over the contact length, the normal force is found:

$$F_N(a) = 2E^* \int_0^a \left[d - g(x)\right] dx = 2E^* \frac{n}{n+1}\kappa_n C a^{n+1} - \sqrt{8\pi a^3 E^* \Delta\gamma}. \tag{4.68}$$

The critical contact radius is obtained from the (transformed) stability equation for the one-dimensional model. It requires only (!) that the profile slope at the contact boundary be known, which is given here by

$$\frac{\partial g(a)}{\partial a} = n\,\kappa_n C a^{n-1}. \tag{4.69}$$

Insertion into (4.23) leads to the critical contact radius

$$\frac{\Delta\ell_{\max}(a_c)}{a_c} = \frac{2}{3} n\,\kappa_n C a_c^{n-1} \;\Rightarrow\; a_c = \left(\frac{9\pi\,\Delta\gamma}{2n^2\kappa_n^2 C^2 E^*}\right)^{\frac{1}{2n-1}}, \tag{4.70}$$

which provides the adhesion force and the critical indentation depth when inserted into the equilibrium relationships:

$$F_c = \frac{1-2n}{n+1}\left[\left(\frac{3}{2n\kappa_n C}\right)^3 (2\pi\,\Delta\gamma)^{n+1} E^{*\,n-2}\right]^{\frac{1}{2n-1}}, \tag{4.71}$$

$$d_c = \left(1 - \frac{2}{3}n\right)\left[\frac{9\pi\,\Delta\gamma}{2n^2 E^*}\left(\frac{1}{\kappa_n C}\right)^{1/n}\right]^{\frac{n}{2n-1}}. \tag{4.72}$$

If normalized by the magnitudes of the critical values $\tilde{F}_N := F_N/|F_c|$, $\tilde{d} := d/|d_c|$, and $\tilde{a} := a/a_c$, the equilibrium relationship exhibit an especially simple structure

$$\tilde{F}_N(\tilde{a}) = \frac{1}{|1-2n|}\left[3\tilde{a}^{n+1} - 2(n+1)\tilde{a}^{3/2}\right] \text{ and } \tilde{d}(\tilde{a}) = \frac{1}{|3-2n|}\left(3\tilde{a}^{n} - 2n\tilde{a}^{1/2}\right). \tag{4.73}$$

For $n = 1$, the results correspond to those from Problem 1, while for $n = 2$, the classical results from JKR theory are obtained. The calculation of the critical contact radius as well as the adhesion force go back to Yao and Gao [25] and were actually employed to investigate adhesion in biological structures [26]. Extended stability considerations can be found in the work by Heß [6].

Problem 4 Determine the normal force and indentation depth with respect to the contact radius for the adhesive normal contact between a sphere with the radius R and an elastic half-space. In contrast to the parabolic profile approximation in JKR theory, the exact spherical form should be considered. Simultaneously, it is assumed that only small deformations take place and the material is linearly elastic.

Solution This contact problem was already solved in Problem 8 in Chap. 3 for the case without adhesion. Referring to this exercise, we can simply take the explicitly calculated equivalent profile:

$$f(r) = R - \sqrt{R^2 - r^2} \Rightarrow g(x) = \frac{1}{2}x\ln\left(\frac{R+x}{R-x}\right). \tag{4.74}$$

By subtracting the separation length from the value of the function of the equivalent profile at the contact boundary, we obtain the indentation depth

$$d(a) = g(a) - \Delta 1_{\max}(a) = \frac{1}{2}a\ln\left(\frac{R+a}{R-a}\right) - \sqrt{\frac{2\pi a\,\Delta\gamma}{E^*}}. \tag{4.75}$$

The displacement in the one-dimensional model is then

$$u_z(x) := d - g(x) = \frac{1}{2}a\ln\left(\frac{R+a}{R-a}\right) - \sqrt{\frac{2\pi a\,\Delta\gamma}{E^*}} - \frac{1}{2}x\ln\left(\frac{R+x}{R-x}\right). \tag{4.76}$$

The calculation of the normal force requires the summation of the contributions from the individual springs and can be immediately given with the help of the solution of the contact without adhesion as

$$F_N(a) = E^*\int_{-a}^{a} u_z(x)\mathrm{d}x = E^*\frac{R^2+a^2}{2}\ln\left(\frac{R+a}{R-a}\right) - E^*Ra - \sqrt{8\pi a^3 E^*\Delta\gamma}. \tag{4.77}$$

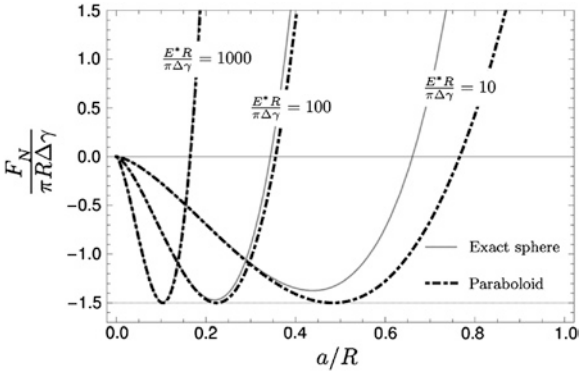

Fig. 4.10 Normal force as a function of contact radius in the normalized presentation for the adhesive contact: Comparison between the parabolic approximation and the exact spherical profile for various values of $m = E^* R/(\pi\,\Delta\gamma)$

By introducing the normalized values $\tilde{F}_N := \frac{F_N}{\pi R\,\Delta\gamma}$ and $\tilde{a} = \frac{a}{R}$ as well as the parameter $m := \frac{E^* R}{\pi\,\Delta\gamma}$, we can convert Eq. (4.77) into the dimensionless form

$$\tilde{F}_N(\tilde{a}) = \frac{1}{2} m \left(1 + \tilde{a}^2\right) \ln\left(\frac{1+\tilde{a}}{1-\tilde{a}}\right) - m\tilde{a} - \sqrt{m}(2\tilde{a})^{3/2}. \tag{4.78}$$

The derived relationships agree exactly to those of the three-dimensional theory developed by Maugis [27]. For comparative purposes, let the respective normalized form of the JKR equation for a parabolic profile be noted:

$$\tilde{F}_N(\tilde{a}) = \frac{4}{3} m\tilde{a}^3 - \sqrt{m}(2\tilde{a})^{3/2}. \tag{4.79}$$

Figure 4.10 emphasizes the difference between the spherical contact and the corresponding parabolic approximation. For large values of the parameter m ($m > 1,000$), they agree well with one another, while for smaller values of m, significant deviations are apparent. The maximum separation force is then especially dependent on the elastic properties. The parabolic approximation appears to give acceptable results over several orders of magnitude of the parameter m up to a contact radius of $a \approx 0.2R$.

With these results, Maugis attempted to describe the contact for small spheres with that of a very soft elastic solid and in this way, proved the invalidity of the parabolic approximation if the contact radius is on the same order of magnitude as the radius of curvature. In this regime, however, the application of the theory of linear elasticity is highly questionable, which Lin and Chen [28] discovered on the basis of geometric and physical *non-linear* theory and for which Greenwood [29] suggested critical additions.

Problem 5 Determine the indentation depth and the normal force as a function of contact radius for the adhesive contact of the axially-symmetric body shown in Fig. 4.11 with an elastic half-space. The form of the body is described by a parabolic profile with a flattened tip:

$$f(r) = \begin{cases} 0 & \text{for } 0 \le r < b \\ \frac{r^2 - b^2}{2R} & \text{for } b \le r \le a \end{cases}. \tag{4.80}$$

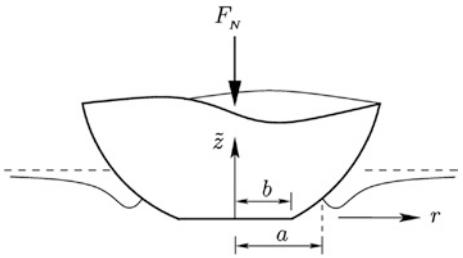

Fig. 4.11 Qualitative presentation of the adhesive contact of a parabolic profile with a flattened tip and an elastic half-space

Solution The corresponding non-adhesive contact problem was solved in Sect. 3.3. It served as an introductory example for the explicit application of the generalized formula (3.27) to determine the equivalent profile, which also composes the first step in the mapping of the contact with adhesion. By taking the derivative of the original profile into account, we obtained

$$g(x) := |x| \int_0^{|x|} \frac{f'(r)}{\sqrt{x^2 - r^2}} \mathrm{d}r = \begin{cases} 0 & \text{for } 0 \le |x| < b \\ \frac{|x|}{R}\sqrt{x^2 - b^2} & \text{for } b \le |x| \le a \end{cases} . \tag{4.81}$$

With the help of (4.81), the indentation depth can be directly given as

$$d(a) := g(a) - \Delta\ell_{\max}(a) = \frac{a}{R}\sqrt{a^2 - b^2} - \sqrt{\frac{2\pi a\,\Delta\gamma}{E^*}}. \tag{4.82}$$

The displacements of the contact points in the linearly elastic foundation are still obtained by the difference between the indentation depth and the value of the equivalent profile and provides the change in length of the spring (with the exception of the sign). Summing the individual spring contributions, leads to the normal force

$$F_N(a) = E^* \int_{-a}^{a} u_z(x)\mathrm{d}x = \frac{2E^*}{3R}\left(2a^2 + b^2\right)\sqrt{a^2 - b^2} - \sqrt{8\pi a^3 E^* \Delta\gamma}. \tag{4.83}$$

The critical values (*fixed load*) in the case of $b = 0$ are those from the original theory for a parabolic body

$$a^* = \left(\frac{9\pi R^2 \Delta\gamma}{8E^*}\right)^{1/3}, \; F^* = -\frac{3}{2}\pi R\,\Delta\gamma\,, \; d^* = -\left(\frac{3\pi^2 R\,\Delta\gamma^2}{64{E^*}^2}\right)^{1/3}, \tag{4.84}$$

which we took from (4.36) and renamed. By normalizing by their magnitudes, we can convert Eqs. (4.82) and (4.83) into the dimensionless forms

$$\hat{d}(\hat{a}) = 3\hat{a}^2\sqrt{1 - \left(\frac{\hat{b}}{\hat{a}}\right)^2} - 4\hat{a}^{1/2}, \tag{4.85}$$

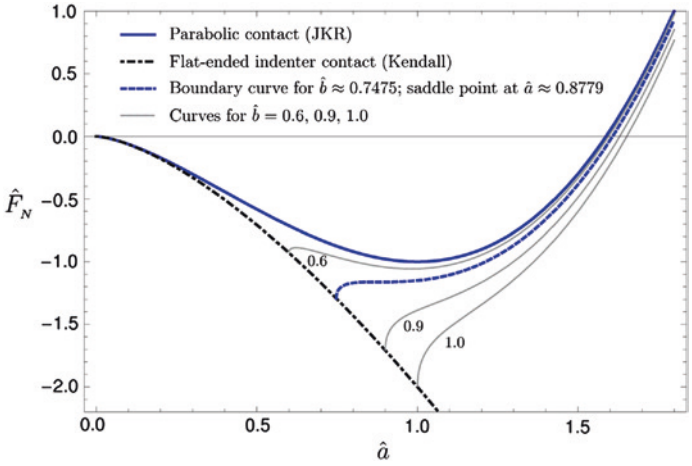

Fig. 4.12 Graphical trends of the normalized normal force as a function of the normalized contact radius for the adhesive contact between a parabolic indenter with a "worn" tip; the parameter b corresponds to the size of the flattened area of the indenter

$$\hat{F}_N(\hat{a}) = \frac{1}{2}\hat{a}^3\left[2 + \left(\frac{\hat{b}}{\hat{a}}\right)^2\right]\sqrt{1 - \left(\frac{\hat{b}}{\hat{a}}\right)^2} - 2\hat{a}^{3/2}, \tag{4.86}$$

where $\hat{F}_N := F_N/|F^*|$, $\hat{d} := d/|d^*|$, $\hat{a} := a/a^*$, and $\hat{b} := b/a^*$ were used for the normalization. In the special case of $\hat{b} = 0$, the resulting equation is (4.38) and for the case of $\hat{b} = \hat{a}$, the resulting equations are (4.61) and (4.62). These cases describe the parabolic contact and the flat indenter contact, respectively. Their graphical trends can be interpreted as extreme values for the general case, which is expressed in Fig. 4.12. Here, unstable domains are not visible. The fact that the horizontal tangents of the minimums of these curves separate the stability domains is clear. It is interesting that for $b > 0.7475\,a^*$, complete separation occurs only after $a = b$, meaning the contact radius corresponds to that of the flattened area of the indenter.

For $b < 0.7475\,a^*$, however, there exists a minimum that marks the adhesion force in a way similar to the parabolic contact. Further considerations, especially those near the boundary curves shown in Fig. 4.12, are contained in [30].

References

1. K.L. Johnson, K. Kendall, A.D. Roberts, Surface energy and the contact of elastic solids. in *Proceedings of the Royal Society of London. Series A, Mathematical and Physical Sciences,* vol. 324, no. 1558 (1971), pp. 301–313
2. B.V. Derjaguin, V.M. Muller, YuP Toporov, Effect of contact deformation on the adhesion of particles. J. Colloid Interface Sci. **55**, 314–326 (1975)
3. R.S. Bradley, The cohesive force between solid surfaces and the surface energy of solids. Philos. Mag. **13**, 853–862 (1932)

4. D. Tabor, Surface forces and surface interactions. J. Colloid Interface Sci. **58**, 2–13 (1977)
5. K.L. Johnson, J.A. Greenwood, An Adhesion Map for the Contact of Elastic Spheres. J. Colloid Interface Sci. **192**, 326–333 (1997)
6. M. Heß, *Über die exakte Abbildung ausgewählter dreidimensionaler Kontakte auf Systeme mit niedrigerer räumlicher Dimension* (Cuvillier, Berlin, 2011)
7. K. Kendall, The adhesion and surface energy of elastic solids. J. Phys. D Appl. Phys. **4**, 1186–1195 (1971)
8. A.A. Griffith, The phenomena of rupture and flow in solids. Philos. Trans. R. Soc. Lond. Ser. A **221**, 163–198 (1921)
9. A.A., Griffith, Theory of rupture. [ed.] Biezeno and Burgers. in *Proceedings of the First International Congress for Applied Mechanics,* 1925, pp. 53–64
10. D. Maugis, M. Barquins, R. Courtel, Griffith Cracks and Adhesion of Elastic Solids. Métaux, Corrosion, Industrie **605**, 1–10 (1976)
11. D. Maugis, M. Barquins, Fracture mechanics and the adherence of viscoelastic bodies. J. Phys. D Appl. Phys. **11**(14), 1989–2023 (1978)
12. G.R. Irwin, Analysis of stresses and strains near the end of a crack traversing a plate. J. Appl. Mech. **24**, 361–364 (1957)
13. Johnson, K.L. Adhesion and friction between a smooth elastic spherical asperity and a plane surface. in *Proceedings of the Royal Society of London. Series A: Mathematical, Physical and Engineering Sciences*, vol. 453, no. 1956. 1997, pp. 163–179
14. D. Maugis, M. Barquins, Adhesive contact of a conical punch on an elastic half-space. Le Journal de Physique Lettres **42**(5), 95–97 (1981)
15. M. Barquins, D. Maugis, Adhesive contact of axisymmetric punches on an elastic half-space: the modified Hertz-Huber's stress tensor for contacting spheres. J. Theor. Appl. Mech. **1**(2), 331–357 (1982)
16. I.N. Sneddon, The relation between load and penetration in the axisymmetric Boussinesq problem for a punch of arbitrary profile. Int. J. Eng. Sci. **3**, 47–57 (1965)
17. K.L. Johnson, A note on the adhesion of elastic solids. British J. Appl. Phys. **9**, 199–200 (1958)
18. D. Maugis, *Contact, adhesion and rupture of elastic solids* (Springer, Berlin, 2000), pp. 213–216
19. M. Heß, On the reduction method of dimensionality: the exact mapping of axisymmetric contact problems with and without adhesion. Phys. Mesomech. **15**(5–6), 264–269 (2012)
20. G.A.D. Briggs, B.J. Briscoe, The effect of surface topography on the adhesion of elastic solids. J. Phys. D Appl. Phys. **10**, 2453–2466 (1977)
21. K.N.G. Fuller, A.D. Roberts, Rubber rolling on rough surfaces. J. Phys. D Appl. Phys. **14**, 221–239 (1981)
22. P.R. Guduru, Detachment of a rigid solid from an elastic wavy surface: Theory. J. Mech. Phys. Solids **55**, 445–472 (2007)
23. P.R. Guduru, C. Bull, Detachment of a rigid solid from an elastic wavy surface: Experiments. J. Mech. Phys. Solids **55**, 473–488 (2007)
24. C. Jin, K. Khare, S. Vajpayee, S. Yang, A. Jagota, C.-Y. Hui, Adhesive contact between a rippled elastic surface and a rigid spherical indenter: from partial to full contact. Soft Matter **7**, 10728–10736 (2011)
25. H. Yao, H. Gao, Optimal shapes for adhesive binding between two elastic bodies. J. Colloid Interface Sci. **298**(2), 564–572 (2006)
26. H. Yao, H. Gao, Mechanical principles of robust and releasable adhesion of gecko. J. Adhes. Sci. Technol. **21**(12–13), 1185–1212 (2007)
27. D. Maugis, Extension of the Johnson-Kendall-Roberts theory of elastic contact of spheres to large contact radii. Langmuir **11**(2), 679–682 (1995)
28. Y.-Y. Lin, H.-Y. Chen, Effect of large deformation and material nonlinearity on the JKR (Johnson-Kendall-Roberts) test of soft elastic materials. J. Polym. Sci. Part B: Polym. Phys. **44**(19), 2912–2922 (2006)
29. J.A. Greenwood, Adhesion of small spheres. Philos. Mag. **89**(11), 945–965 (2009)
30. D. Maugis, M. Barquins, Adhesive contact of sectionally smooth-ended punches on elastic half-spaces: theory and experiment. J. Phys. D Appl. Phys. **16**(10), 1843–1874 (1983)